Journal of Stroke and Cerebrovascular Diseases 32 (2023) 107357

Contents lists available at ScienceDirect

Journal of Stroke and Cerebrovascular Diseases

journal homepage: www.elsevier.com/locate/jstroke

Clinical potential of automated convolutional neural network-based hematoma volumetry after aneurysmal subarachnoid hemorrhage☆

Bart R Thomson [a,b,#], Firat Gürlek [a,b,#], Raphael M Buzzi [b], Nina Schwendinger [a], Emanuela Keller [a,c], Luca Regli [a], Tristan PC van Doormaal [a,d,e], Dominik J Schaer [b], Michael Hugelshofer [a], Kevin Akeret [a,*]

[a] Department of Neurosurgery, Clinical Neuroscience Center, Universitätsspital und University of Zurich, Rämistrasse 100, Zurich CH-8091, Switzerland
[b] Division of Internal Medicine, Universitätsspital and University of Zurich, Zurich, Switzerland
[c] Neurointensive Care Unit, Department of Neurosurgery, and Institute of Intensive Care Medicine, Universitätsspital and University of Zurich, Zurich, Switzerland
[d] Department of Neurology and Neurosurgery, University Medical Center Utrecht, Utrecht, The Netherlands
[e] Department of Translational Neuroscience, University Medical Center Utrecht, Brain Center, Utrecht University, Utrecht, The Netherlands

ARTICLE INFO

Keywords:
Secondary brain injury
Angiographic vasospasm
Delayed cerebral ischemia
Delayed ischemic neurologic deficit
Hemoglobin
Imaging

ABSTRACT

Objectives: Cerebrospinal fluid hemoglobin has been positioned as a potential biomarker and drug target for aneurysmal subarachnoid hemorrhage-related secondary brain injury (SAH-SBI). The maximum amount of hemoglobin, which may be released into the cerebrospinal fluid, is defined by the initial subarachnoid hematoma volume (ISHV). In patients without external ventricular or lumbar drain, there remains an unmet clinical need to predict the risk for SAH-SBI. The aim of this study was to explore automated segmentation of ISHV as a potential surrogate for cerebrospinal fluid hemoglobin to predict SAH-SBI.

Methods: This study is based on a retrospective analysis of imaging and clinical data from 220 consecutive patients with aneurysmal subarachnoid hemorrhage collected over a five-year period. 127 annotated initial non-contrast CT scans were used to train and test a convolutional neural network to automatically segment the ISHV in the remaining cohort. Performance was reported in terms of Dice score and intraclass correlation. We characterized the associations between ISHV and baseline cohort characteristics, SAH-SBI, ventriculoperitoneal shunt dependence, functional outcome, and survival. Established clinical (World Federation of Neurosurgical Societies, Hunt & Hess) and radiological (modified Fisher, Barrow Neurological Institute) scores served as references.

Results: A strong volume agreement (0.73 Dice, range 0.43 - 0.93) and intraclass correlation (0.89, 95% CI, 0.81-0.94) were shown. While ISHV was not associated with the use of antithrombotics or cardiovascular risk factors, there was strong evidence for an association with a lower Glasgow Coma Scale at hospital admission. Aneurysm size and location were not associated with ISHV, but the presence of intracerebral or intraventricular hemorrhage were independently associated with higher ISHV. Despite strong evidence for a positive association between ISHV and SAH-SBI, the discriminatory ability of ISHV for SAH-SBI was insufficient. The discriminatory ability of ISHV was, however, higher regarding ventriculoperitoneal shunt dependence and functional outcome at three-months follow-up. Multivariate survival analysis provided strong evidence for an independent negative association between survival probability and both ISHV and intraventricular hemorrhage.

Abbreviations: aSAH, aneurysmal subarachnoid hemorrhage; AUC, area under the curve; aVSP, angiographic vasospasm; BNI, Barrow Neurological Institute; CNN, convolutional neural network; CSF, cerebrospinal fluid; CSF-Hb, cell-free hemoglobin in the cerebrospinal fluid hemoglobin; DCI, delayed cerebral ischemia; DIND, delayed ischemic neurologic deficits; GAM, generalized additive model; GCS, Glasgow Coma Scale; ICC, intraclass correlation; ISHV, initial subarachnoid hematoma volume; mRS, modified Rankin Scale; PD, partial dependence; ROC, receiver operating characteristic; SAH-SBI, subarachnoid hemorrhage related secondary brain injury; WFNS, World Federation of Neurosurgical Societies.

☆ Phone numbers of authors: Thomson: +41 44 255 11 11; Gürlek: +41 44 255 11 11; Buzzi: +41 44 255 11 11; Schwendinger: +41 44 255 11 11; Keller: +41 44 255 11 11; Regli: +41 44 255 11 11; Doormaal: +41 44 255 11 11; Schaer: +41 44 255 11 11; Hugelshofer: +41 44 255 11 11; Akeret: +41 44 255 11 11.
* Corresponding author.
E-mail address: kevin.akeret@usz.ch (K. Akeret).
# These authors contributed equally to this work.

https://doi.org/10.1016/j.jstrokecerebrovasdis.2023.107357
Received 8 June 2023; Received in revised form 8 September 2023; Accepted 11 September 2023
Available online 19 September 2023
1052-3057/© 2023 The Author(s). Published by Elsevier Inc. This is an open access article under the CC BY license (http://creativecommons.org/licenses/by/4.0/).

Conclusions: The proposed algorithm demonstrates strong performance in volumetric segmentation of the ISHV on the admission CT. While the discriminatory ability of ISHV for SAH-SBI was similar to established clinical and radiological scores, it showed a high discriminatory ability for ventriculoperitoneal shunt dependence and functional outcome at three-months follow-up.

Introduction

Aneurysmal subarachnoid hemorrhage (aSAH) has an incidence of 5-10/100'000 person-years and accounts for 5-10% of all strokes .[1,2] Brain damage resulting from the initial hemorrhage and within the first 72 hours is referred to as early brain injury [3]. The functional outcome of patients after aSAH is, however, strongly determined by the occurrence and extent of aSAH-related secondary brain injury (SAH-SBI) [4]. SAH-SBI has a delayed manifestation, characteristically between day 4 and day 14 after aSAH [4]. Within this time window, two-thirds of patients develop angiographic vasospasm of the large cerebral arteries (aVSP) [5] and one-third demonstrates delayed cerebral ischemia (DCI) with radiological demarcation of ischemic brain areas or delayed ischemic neurologic deficits (DIND) [6]. The diagnosis of at least one of these delayed secondary manifestations defines SAH-SBI [7]. While in recent decades significant advances have been made in the acute care of patients with aSAH, there has been little progress in the prediction, prevention, and therapy of SAH-SBI. [4]

The delayed onset of SAH-SBI with a latency of 4 to 14 days after aneurysm rupture would provide a unique window-of-opportunity for preventive therapies. Cell-free hemoglobin in the cerebrospinal fluid (CSF-Hb) may be a suitable target molecule [7–9]. CSF-Hb levels rise with a latency of several days after aSAH as a result of delayed red blood cell lysis, and there is strong clinical evidence for a positive association between CSF-Hb levels and SAH-SBI .[7,10] In preclinical studies, cell-free Hb in the clinically relevant concentration range has been identified as a pathophysiological driver of processes that reflect specific features of SAH-SBI, such as vasoconstrictive or oxidative damage. [7,8,11,12] Haptoglobin is a phylogenetically preserved plasma protein that acts as a scavenger of cell-free hemoglobin to protect against its toxicity after intravascular lysis. [13–15] In ex vivo assays and large animal models, the intraventricular application of haptoglobin was shown to protect against aVSP by scavenging CSF-Hb [7,8] The indication for such an invasive preventive therapy would have to be tailored to the patients' risk profile for SAH-SBI. Daily CSF-Hb measurement seems to have a high discriminatory ability for SAH-SBI and could in the future serve as a monitoring biomarker. [7,16] This, however, requires a cerebrospinal fluid (CSF) diversion device, i.e., external ventricular drain or lumbar drain. These are invasive procedures with strict indications. Thus, there is an unmet clinical need in patients without a CSF diversion device to predict the risk for SAH-SBI, functional outcome, and survival.

The initial subarachnoid hematoma volume (ISHV) could serve as a surrogate biomarker for CSF-Hb, since CSF-Hb was shown to have a positive linear association with the ISHV [7]. This implies a potential association between ISHV and the occurrence of SAH-SBI, ventriculoperitoneal shunt dependence, functional outcome, and survival [7]. Manual volumetry of ISHV does not lend itself for integration into daily clinical practice given its time-consuming nature [17]. However, the performance of deep learning methods, in particular convolutional neural networks (CNNs), has made near human performance possible in numerous medical imaging challenges [18], including the segmentation of subarachnoid hematomas [19]. These novel methods facilitate automatic volume measurements in a clinical setting, warranting further investigation of their potential.

The aim of this study was to develop and validate an automated CNN-based ISHV segmentation algorithm and to evaluate its clinical potential. We characterized the associations between ISHV and baseline cohort characteristics, SAH-SBI within the first two weeks after hemorrhage, ventriculoperitoneal shunt dependence, functional outcome at three months follow-up, and survival. Established clinical [20,21] and radiological scores [22–24] served as reference values.

Methods

This study was approved by the ethical review board of the Canton of Zurich, Switzerland (KEK ZH 2021-01844). A written general consent for further use of their patient-specific data has been obtained from all patients or their legal representatives. The results are reported in accordance with the STROBE statement. [25]

Study population

This study is based on a retrospective analysis of prospectively collected clinical data from the Department of Neurosurgery, Universitätsspital Zürich, Zurich, Switzerland. We included adult (≥18 years) patients with aSAH, admitted to the hospital over a five-year period (between January 1, 2016, and December 31, 2020). Patients with nonaneurysmal subarachnoid hemorrhage (e.g., trauma, perimesencephalic, no evidence of an aneurysm on angiography) were not included in the analysis.

Data acquisition

Imaging and clinical data was acquired in one of the following phases: hospital admission, monitoring period (day 0 to day 14 after aneurysm rupture (day post-SAH), i. e., the high-risk phase for SAH-SBI), three-month follow-up, and last known follow-up (Fig. 1).

Image data

In all patients, we used the initial CT scan for image segmentation and volumetry. This data originated either from our hospital or from an external referrer. The technical specifications regarding image acquisition varied accordingly. For image processing, the encoded original non-contrast dataset was exported as DICOM.

Patient baseline characteristics

Baseline characteristics were assessed at the time of patient hospital admission. These included demographics (age, sex), aneurysm characteristics (maximum diameter, anatomic location), presence of intraparenchymal or intraventricular blood, past medical history (use of antithrombotics/anticoagulants, diabetes, hypertension, coronary artery disease, smoking status), symptoms and neurological status at admission (pupil status, cranial nerve deficits, focal neurological deficits), clinical scores (Glasgow Coma Scale (GCS), World Federation of Neurosurgical Societies (WFNS), Hunt & Hess), radiological scores (modified Fisher, Barrow Neurological Institute (BNI)), and aneurysm treatment. In addition, it was assessed whether patients required a CSF diversion device (external ventricular drain or lumbar drain) at any time during hospitalization.

SAH-SBI, aVSP, DCI, and DIND

During the monitoring phase (day 0-14 post-SAH) the occurrence of SAH-SBI, aVSP, DCI, and DIND was evaluated every day. Each of the assessments referred to the past 24 hours and were based on clinical examinations performed several times a day in our neurosurgical intensive care unit and imaging procedures (CT angiography / CT perfusion, MRI / MR angiography, digital subtraction angiography). SAH-SBI represents a composite outcome of aVSP, DCI, and DIND. DIND

is defined as a new focal neurologic deficit or a decrease in GCS of at least 2 points for at least 2 hours. If the patient could not be assessed clinically (e.g., sedation), this was noted as not assessable. DCI is defined as new ischemia or new infarction on CT/CTP or MRI. If no corresponding imaging procedure was performed on that day, it was noted as imaging not performed. The definition of aVSP includes narrowing of cerebral arteries based on digital subtraction angiography, CT angiography, or MR angiography. If no corresponding imaging procedure was performed on that day, it was noted as imaging not performed.

Spasmolysis

During the monitoring phase (day 0-14 post-SAH), it was also recorded daily whether a rescue therapy with pharmacological spasmolysis or balloon angioplasty was performed within the last 24 hours.

Three-months and last-known follow-up

Based on the three-months follow-up (outpatient or inpatient depending on the patient's condition), the functional status (modified Rankin Scale (mRS)) and dependence on a ventriculoperitoneal shunt (i.e., chronic hydrocephalus) were assessed. Overall survival was assessed based on the time (in days) from aneurysm rupture until death or last follow-up (censored).

Image segmentation

CNN-based ISHV segmentation

No additional preprocessing was performed on the acquired imaging, to prevent potential misinterpretation of data. The ground truth segmentations of the initial subarachnoid hematoma were manually delineated by one of two experienced observers and controlled by a neurosurgeon. The proposed segmentation model was based on a 3D UNet architecture with residual units [26], developed using the MONAI framework, which is a freely available, open source framework for deep learning in healthcare imaging [27]. This architecture was chosen due to the improved robustness against input with divergent appearance from the training data [26]. A grid search was used to optimize the hyperparameters (Table 1) of the proposed CNN, in which the Dice score was used as a selection criterion. The best performing model had 5 layers with 16, 32, 64, 128 and 256 channels respectively, 2 residual units and a stride of 2 in all dimensions (Fig. 2A). During the training process (on an NVIDIA Tesla K80 GPU), 96×96×96 voxel input patches were clipped between 0 and 300 Hounsfield units for normalization purposes, followed by random zooming, rotating, and flipping along all axes. Additionally, random gaussian smoothing and noise were applied. Dice loss with the Adam optimizer was used with a learning rate of 0.001, without weight decay.

Table 1
Hyperparameters used during optimization of the proposed CNN via grid search.

Hyper parameter	Evaluated values
Number of convolutional layers	4 or 5
Feature maps in the convolutional layers	[16, 32, 64, 128], [32, 64, 128, 256], [16, 32, 64, 128, 256] or [32, 64, 128, 256, 512]
Loss function	Dice loss or Focal loss
Learning rate	0.001 or 0.0001
Batch size	1 or 2
Size of input patch	96×96×96, 104×104×104 or 112×112×112

Volumetry

A total of 127 initial scans after aSAH were used in training of the CNN, split into 69, 13 and 45 scans in respectively the training, validation, and test set. The scans that were used as ground truth were randomly selected from patients included in the current study, as well as from a period prior to the study. A neurosurgeon judged these volumes to be clinically representable and sufficiently varied. Following selection of the best performing model on the test set, blood volume was calculated by multiplying the amount of automatically segmented voxels by the voxel volume. Performance is reported in terms of Dice score, 95% Hausdorff distance (95%HD) and intraclass correlation (ICC).

Statistical analysis

All statistical analyses were performed using the statistical software R 4.1.1 (R Core Team, 2022) in the RStudio environment (V 1.3.1093). For descriptive statistics, continuous variables were reported as mean and standard deviation (SD), categorical variables as absolute numbers (n) and proportions (%) with a 95% Wilson confidence interval. Missing data was considered as separate category and assessed for non-randomness. The strength of association between ISHV (dependent continuous variable) and clinical or radiological baseline data (independent binary or continuous variables) was assessed based on multiple linear regression. The strength of association between SAH-SBI (dependent binary variable) and ISHV (independent continuous variable) was estimated based on a generalized additive model (GAM) with day post-SAH as a covariate (nonlinear spline fit) and repeated observations in the same patients over time accounted for with random intercepts (mgcv package v1.8-31 [28]). The discriminatory ability of ISHV for SAH-SBI, aVSP, DCI, DIND, ventriculoperitoneal shunt dependence, and functional status was analyzed using receiver operating characteristic (ROC) curves (ROCR package (v1.0-11), [29] plotROC package (v2.2.1) [30]), the corresponding bootstrap area under the curves (AUC) (pROC package (v1.16.2) [31]) and the optimal Youden indices (ROCit package (v1.1.1) [32]). The Kaplan Meier method was used to plot survival probabilities and pairwise comparisons between subgroups were

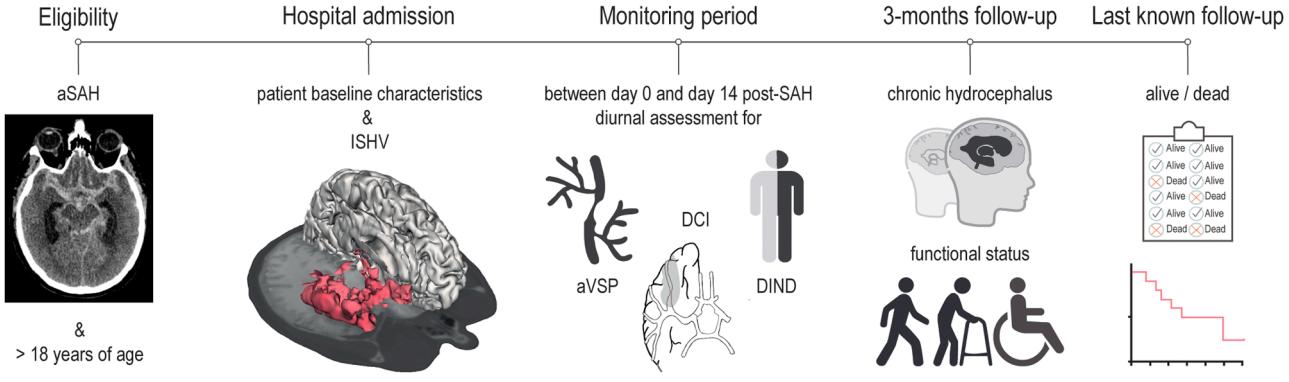

Fig. 1. Data acquisition. Schematic depiction of the different phases of clinical and image data acquisition. aSAH, aneurysmal subarachnoid hemorrhage; aVSP, angiographic vasospasms; DCI, delayed cerebral ischemia; DIND, delayed ischemic neurological deficits; ISHV, initial subarachnoid hematoma volume; SAH-SBI, subarachnoid hemorrhage-related secondary brain injury.

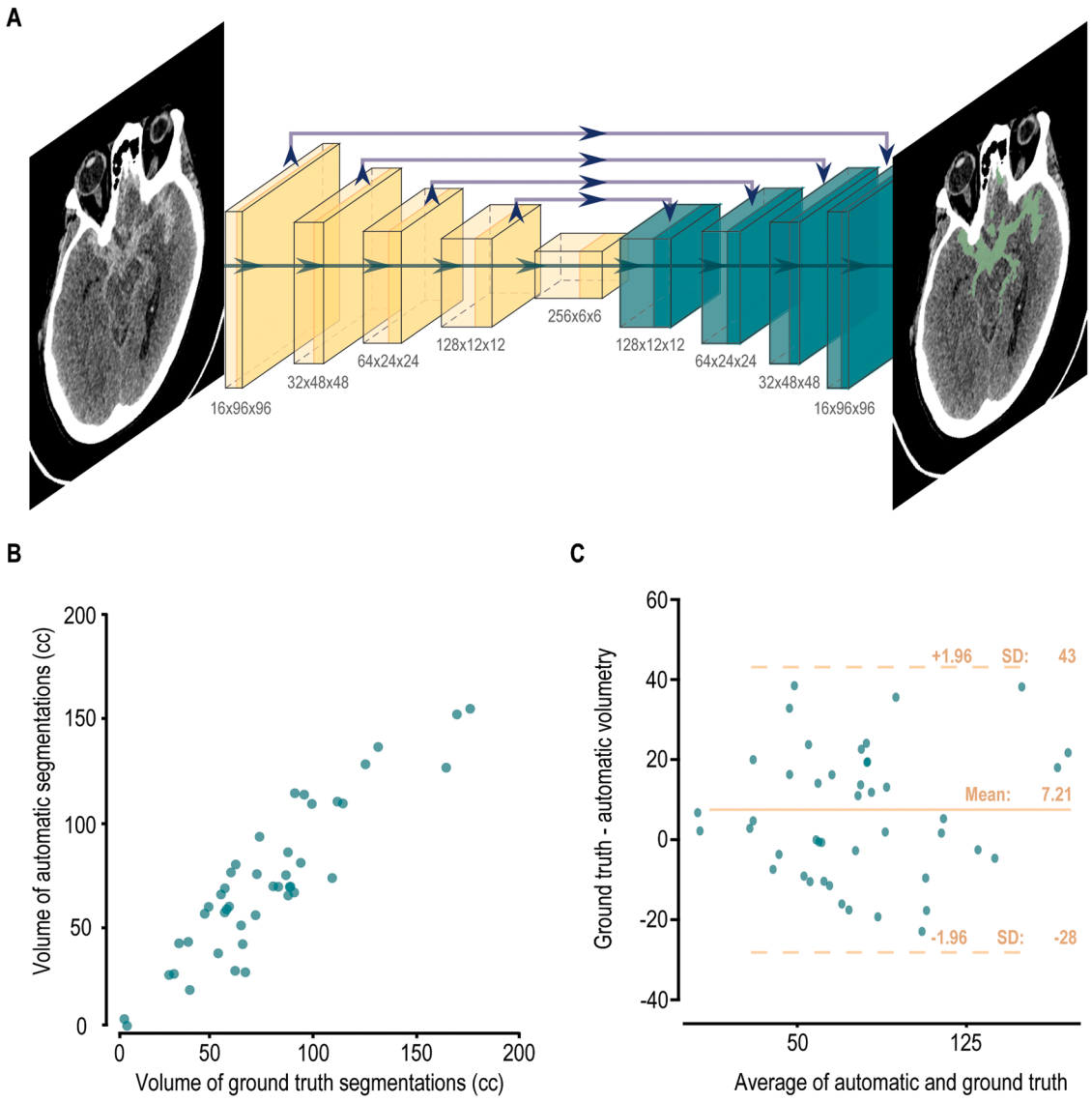

Fig. 2. Architecture and performance statistics of the proposed convolutional neural network. (**A**) Visualization [58] of the UNet architecture that is used in automatic segmentation of the aSAH volumes. (**B**) Scatterplot presenting the accuracy of volume measurement of the automatic method compared to the ground truth. (**C**) Bland-Altman plot of the averages and differences between the ground truth and the automatic method in cc.

performed using the log-rank test with Bonferroni-Holm correction for multiple testing across discriminatory tasks [33]. The Cox proportional hazards regression model served for multivariable survival analysis. [34] No statistical significance levels were defined for the analyses in this study due to their exploratory nature. Instead, results are interpreted based on the level of evidence: $p < 0.001$: very strong evidence; $p < 0.01$: strong evidence; $p < 0.05$ evidence; $p < 0.1$ weak evidence; $p > 0.1$: no evidence. [35]

Results

The study cohort contained 220 patients, with a mean age of 57.8 years (SD 12.7 years) and female predominance (65.0%). Detailed cohort characteristics are presented in Table 2.

Performance of CNN-based automated volumetry

Our CNN demonstrated strong volume agreement regarding both the volumetric overlap (Dice score of 0.73, SD 0.11, ranging from 0.43 to 0.93 and 95%HD of 9.5 voxels, SD 5.5, ranging from 1.5 to 26.7), and ICC (0.89, 95% CI, 0.81-0.94) in the test set. Mean ISHV across the entire cohort was 55.3 cc (SD 39.0 cc). The mean segmented volumes in the test set were 80.5 cc (SD 41.1 cc) for manual segmentation and 73.3 cc (SD 36.8 cc) for the CNN-based segmentation (Fig. 2B). Bland-Altman analysis showed a bias of 7.21 cc, indicating slight under-segmentation of the CNN. There was a relatively large spread with the 95% limits of agreement between -28 and 43 cc (Fig. 2C). This spread becomes apparent in the overlap when individual automated segmentations are observed (Fig. 3), where higher reliability is achieved in patients with larger hematoma volumes.

Associations between ISHV and clinical baseline parameters

The relation of ISHV to sex and age is visualized in Fig. 4A. There was no evidence for an association between ISHV and the intake of anti-platelets (partial dependence (PD) -4.3, SE 8.6, $p = 0.62$), anticoagulants (PD 11.5, SE 16.3, $p = 0.48$), or a combination of both (PD -42.8, SE 41.8, $p = 0.31$) (Fig. 4B). In the same model, there was no evidence for an association between ISHV and a history of hypertension (PD 9.4, SE 5.7, $p = 0.10$), diabetes (PD 9.8, SE 12.2, $p = 0.42$), coronary artery

Table 2
Demographic, clinical, and radiological cohort features.

Total *n*	220	4	37 (16.8)
Male gender [*n* (%)]	77 (35.0)	5	74 (33.6)
Age (mean (SD))	57.8 (12.7)	Hunt and Hess grade [n (%)]	
Aneurysm location [*n* (%)]		1	36 (16.4)
Middle cerebral artery	68 (30.9)	2	50 (22.7)
Anterior communicating artery	69 (31.4)	3	32 (14.5)
Posterior communicating artery	25 (11.4)	4	52 (23.6)
Internal carotid artery	17 (7.7)	5	50 (22.7)
Anterior cerebral artery	11 (5.0)	mFisher grade [*n* (%)]	
Posterior inferior cerebellar artery	9 (4.1)	1	15 (6.8)
Basilar-tip artery	7 (3.2)	2	4 (1.8)
Miscellaneous	14 (6.4)	3	109 (49.5)
Aneurysm size[a] [mean (SD)]	8.1 (5.5)	4	92 (41.8)
Intracerebral hemorrhage [*n* (%)]	93 (42.3)	BNI grade [*n* (%)]	
Intraventricular hemorrhage [*n* (%)]	92 (41.8)	1	5 (2.3)
AP/AC before admission [*n* (%)]		2	34 (15.5)
None	185 (84.1)	3	47 (21.4)
AP	28 (12.7)	4	50 (22.7)
AC	6 (2.7)	5	84 (38.2)
AP and AC	1 (0.5)	Aneurysm treatment [*n* (%)]	
Smoking [*n* (%)]		None	16 (7.3)
Never	144 (65.5)	Bypass	9 (4.1)
Current	62 (28.2)	Clipping	110 (50.0)
Quitted	12 (5.5)	Coiling	81 (36.8)
Missing data	2 (0.9)	Flow diverter	1 (0.5)
GCS [mean (SD)]	9.4 (5.3)	Others	3 (1.4)
WFNS grade [*n* (%)]		CSF diversion device [*n* (%)]	
1	63 (28.6)	No EVD/LD	51 (23.2)
2	34 (15.5)	EVD	143 (65.0)
3	12 (5.5)	LD	26 (11.8)

[a]Maximal diameter in mm.
SD: Standard deviation; AP: Antiplatelet; AC: Anticoagulant; GCS: Glasgow Coma Scale; WFNS: World Federation of Neurosurgical Societies; mFisher: Modified Fisher Scale; Barrow Neurological Institute; CSF: Cerebrospinal fluid; EVD: External ventricular drain; LD: Lumbar drain

disease (PD 4.0, SE 14.6, $p = 0.78$), or smoking (*current smoker:* PD -8.2, SD 6.2, $p = 0.18$; *missing data on smoking:* PD 24.8, SE 27.5, $p = 0.37$). There was, however, evidence for an association between ISHV and specific clinical features at hospital admission. ISHV increased with higher Hunt & Hess and WFNS scores (Fig. 4C). More specifically, ISHV had an inverse association to the patient's GCS ($p < 0.001$) (Fig. 4D). In addition, there was some evidence for a positive association between ISHV and having quit smoking (quitted smoking: PD -28.4, SE 11.9, p = 0.02). There was, however, no evidence for an association between ISHV and cranial nerve deficits (*cranial nerve deficits:* PD 7.2, SE 11.0, $p = 0.52$; *missing data:* PD 14.9, SE 10.9, $p = 0.17$), the patient's pupil status at hospital admission (bilateral mydriasis: PD 28.5, SE 16.6, p = 0.09; anisocoria: PD 7.0, SE 7.3, p = 0.34; missing pupil status: PD -18.6, SE 32.6, p = 0.57) or other focal neurological deficits (*motor deficits:* PD 8.2, SE 11.1, $p = 0.46$; *sensory deficits:* PD 32.9, SE 34.1, $p = 0.34$; *motor and sensory deficits:* PD -4.4, SE 10.4, p = 0.67; *missing data:* PD -20.7, SE 11.65, $p = 0.08$. Collectively, while the ISHV was not associated with the use of antithrombotics and cardiovascular risk factors, there was strong evidence for an association to a lower GCS at hospital admission.

Associations between ISHV and radiological baseline features

Mean ISHV increased along BNI grades (Fig. 5A). ISHV was highest with modified Fisher grades 2 and 4, intermediate with modified Fisher grade 3, and lowest with modified Fisher grade 1 aSAH (Fig. 5B). There was strong evidence that both the presence of intracerebral hemorrhage (PD 20.4, SE 5.1, $p < 0.001$) and intraventricular hemorrhage (PD 28.6, SE 5.0, $p < 0.0001$) are independent factors positively associated with ISHV, while there was no evidence for an association between ISHV and aneurysm size ($p = 0.33$) or aneurysm location (*Anterior communicating artery:* PD 2.4, SE 6.0, $p = 0.69$ *Posterior communicating artery:* PD 2.74; SE 8.1; $p = 0.74$; *Internal carotid artery:* PD 0.19, SE 9.2, $p = 0.98$; *Anterior cerebral artery:* PD 4.12, SE 11.1, $p = 0.71$; *Posterior inferior cerebellar artery:* PD -5.9, SE 12.6, $p = 0.64$; *Basilar tip:* PD -3.7, SE 13.7, $p = 0.79$; *Miscellaneous:* PD -9.9, SE 10.3, $p = 0.34$) (Fig. 5C).

Discriminatory ability of ISHV for SAH-SBI

Overall, 55.5% of the patients in this cohort endured aVSP at some point during the monitoring phase (day 0-14 post-SAH), DCI was diagnosed in 23.6%, and 17.7% developed DIND (Table 3). Spasmolysis was performed in 16.4% of patients. The results of diurnal assessment for aVSP, DCI, DIND are presented in Fig. 6A and summarized in Table 4.

The strength of association between SAH-SBI and ISHV was estimated based on a GAM with day post-SAH as a nonlinear covariate and repeated observations in the same patients over time accounted for with random intercepts (Fig. 6B). There was strong evidence ($p_{ISHV} < 0.01$) for a positive association between SAH-SBI and ISHV ($p_{Day\ post\text{-}SAH} < 0.0001$, $p_{Patient\ ID} < 0.0001$). Separate GAM-based analyses on the associations between aVSP, DCI, and DIND with ISHV are provided in Supplementary Figure 1.

We assessed the discriminatory ability of ISHV for the occurrence of SAH-SBI, aVSP, DCI, and DIND at any time-point during the monitoring phase based on ROC analyses (Fig. 6C). The areas under the curves were $AUC_{SAH\text{-}SBI} = 0.51$ (0.43-0.59), $AUC_{aVSP} = 0.52$ (0.44-0.60), $AUC_{DCI} = 0.51$ (0.43-0.60), and $AUC_{DIND} = 0.46$ (0.38-0.55). The optimal Youden indices were 22.1 cc for SAH-SBI, 22.1 cc for aVSP, 28.1 cc for DCI, and 73.7 cc for DIND. As references, we determined the discriminatory ability of established clinical (WFNS, Hunt & Hess) and radiological (modified Fisher, BNI) scores for SAH-SBI, aVSP, DCI, and DIND (Fig. 6D & Table 5).

Discriminatory ability of ISHV for ventriculoperitoneal shunt dependence

Fig. 7A displays ISHV stratified by the patient's dependence on a ventriculoperitoneal shunt three months after aSAH. Mean ISHV was 41.1 cc (SD 3.9 cc) in patients without shunt dependence after three months, 56.7 cc (SD 4.2 cc) in patients with shunt dependence, and 79.5 cc (SD 5.5 cc) in those that died before the three-months follow-up. We found evidence that ventriculoperitoneal shunt dependence is associated with higher ISHV ($p < 0.01$). In addition, we assessed the discriminatory ability of ISHV for ventriculoperitoneal shunt dependence after three months based on ROC analyses (Fig. 7B), resulting in an area under the curve of 0.65 (0.56-0.74). This was comparable to the discriminatory ability found with established clinical ($AUC_{WFNS} = 0.69$ (0.61-0.78), $AUC_{Hunt\&Hess} = 0.71$ (0.63-0.79)) and slightly above the area under the curves of radiological ($AUC_{modified\ Fisher} = 0.58$ (0.49-0.66), $AUC_{BNI} = 0.53$ (0.44-0.63)) scores (Supplementary Figure 2).

Discriminatory ability of ISHV for functional status after three months

ISHV stratified by mRS after three months is shown in Fig. 8A. A higher mRS was associated with a larger ISHV (Mean $ISHV_{mRS\ 0} = 34.2$ cc (SD 4.6 cc), Mean $ISHV_{mRS\ 1} = 33.4$ cc (SD 4.7 cc), Mean $ISHV_{mRS\ 2} = 45.9$ cc (SD 5.9), Mean $ISHV_{mRS\ 3} = 58.3$ cc (SD 6.2 cc), Mean $ISHV_{mRS\ 4} = 68.1$ cc (SD 8.9 cc), Mean $ISHV_{mRS\ 5} = 74.4$ cc (SD 11.1 cc), Mean

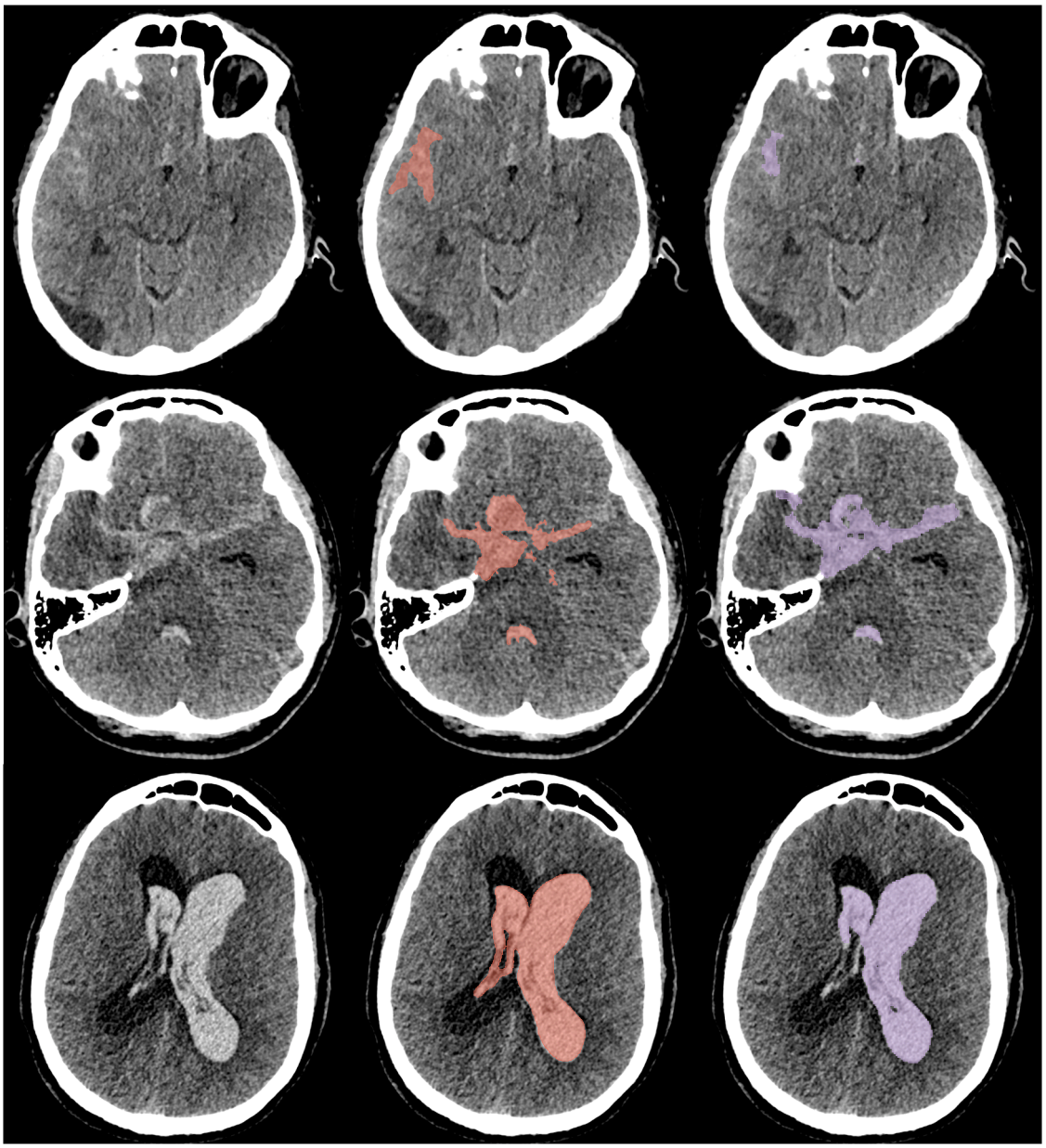

Fig. 3. Representative examples comparing input CT scan, ground truth and automated segmentation for different Dice coefficients. All scans are visualized with the display window (W:100, L:50). First column: Input CT scan. Second column: Ground truth. Third column: Automated segmentation. First row: Dice coefficient of 0.43. Second row: Dice coefficient of 0.72. Third row: Dice coefficient of 0.92.

$ISHV_{mRS\ 6}$ = 79.5 cc (SD 5.5 cc)). The area under the receiver operating characteristic curve of the ISHV discriminating between a good (0-2) and a poor (3-6) mRS three months after hemorrhage was 0.78 (0.72-0.84) (Fig. 8B). This was comparable to the discriminatory ability of established clinical (AUC_{WFNS} = 0.81 (0.75-0.87), $AUC_{Hunt\&Hess}$ = 0.80 (0.74-0.86)) and slightly superior to radiological scores ($AUC_{modified\ Fisher}$ = 0.69 (0.63-0.76), AUC_{BNI} = 0.57 (0.49-0.64)) (Supplementary Figure 3).

Survival after aSAH in relation to the ISHV

We performed a multivariate survival analysis considering WFNS grade, presence of intraventricular hemorrhage, presence of intracerebral hemorrhage, and ISHV (Fig. 9A). There was evidence for a negative association between ISHV and survival probability (p = 0.01). In addition, there was evidence for a negative association of survival probability with WFNS grade ($HR_{WFNS\ 5}$ = reference, $HR_{WFNS\ 4}$ = 0.96 (0.52-1.78, p = 0.91), $HR_{WFNS\ 3}$ = 0.68 (0.20-2.26, p = 0.53), $HR_{WFNS\ 2}$ = 0.37 (0.15-0.92, p = 0.03), $HR_{WFNS\ 1}$ = 0.43 (0.18-1.05, p = 0.06)) and a negative association with the presence of intraventricular hemorrhage (HR = 2.23 (1.27-3.90, p = *0.005*)). There was, however, no evidence for an independent association between the presence of intracerebral hemorrhage and survival probability (HR = 0.73 (0.44-1.22, p = 0.23)). Survival probability stratified by the optimal discriminatory (optimal Youden indices) of ISHV for aVSP (22.1 cc), DCI (28.1 cc), and DIND (73.7 cc), was visualized using the Kaplan Meier method (Fig. 9B and Supplementary Figure 4).

Discussion

Our automated CNN-based ISHV segmentation method demonstrated strong performance regarding both volumetry and ICC. While cardiovascular risk factors and the use of antithrombotics showed no association to the ISHV, there was an inverse association to the GCS at

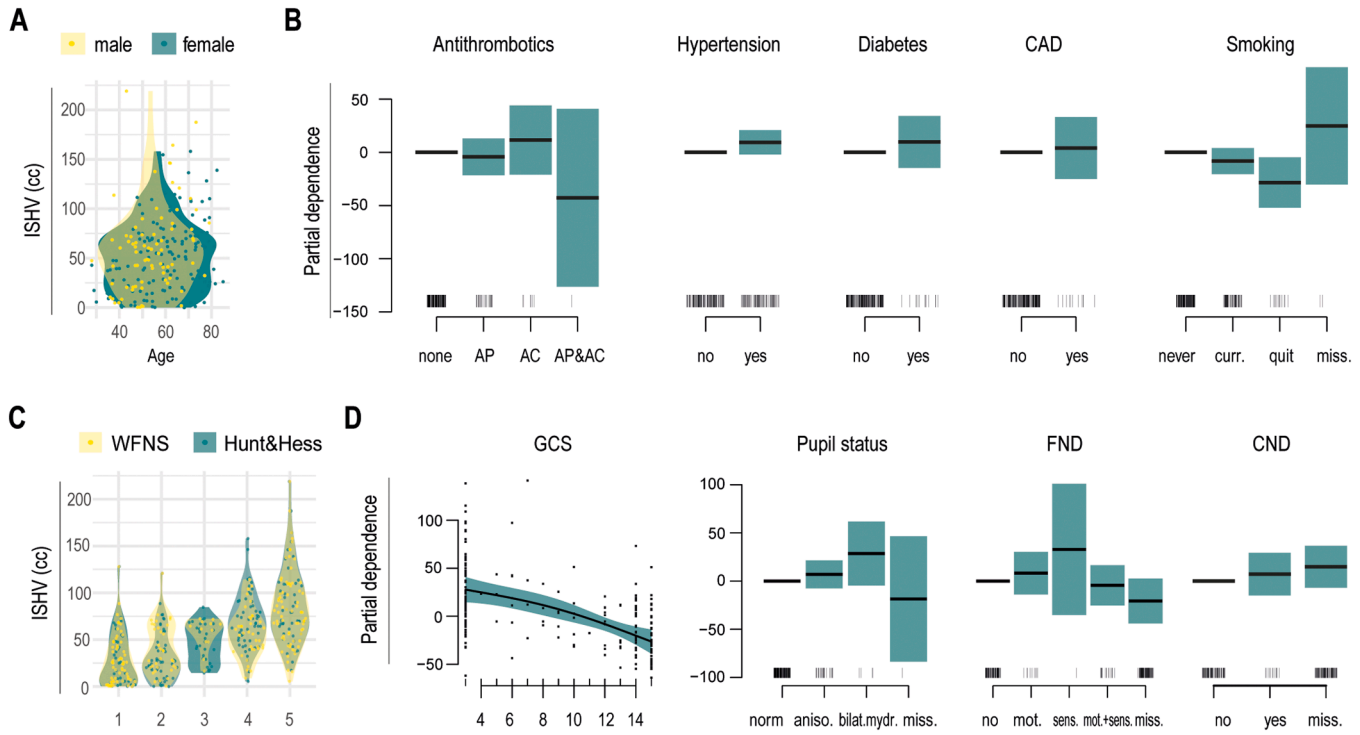

Fig. 4. Initial subarachnoid hematoma volume and clinical baseline parameters. (**A**) Initial subarachnoid hematoma volume (ISHV) in relation to sex and age. (**B**) Partial dependence of the ISHV on antithrombotics (none, antiplatelets (AP), anticoagulants (AC), or both), hypertension, diabetes, coronary artery disease (CAD), and smoking status. (**C**) ISHV in relation to established clinical aSAH scores (Hunt & Hess, World Federation of Neurosurgical Societies (WFNS)). (**D**) Partial dependence of ISHV on Glasgow Coma Scale (GCS), pupil status, functional neurologic deficits (FND), and cranial nerve deficits (CND).

hospital admission. Aneurysm size and location were not associated with the ISHV, but the presence of intracerebral or intraventricular hemorrhage were independently associated with higher ISHV. Despite strong evidence for a positive association between ISHV and SAH-SBI, the discriminatory ability of ISHV for SAH-SBI was insufficient. The discriminatory ability of ISHV was, however, higher regarding ventriculoperitoneal shunt dependence and functional outcome at three-months follow-up. Multivariate survival analysis provided strong evidence for an independent negative association between survival probability and both ISHV and intraventricular hemorrhage.

While there are several previously described segmentation approaches to intracranial hemorrhage [17,36–39], only two were tested on aSAH in 3D. [19,40] Our CNN with a Dice score of 0.73 (SD 0.11) and an ICC of 0.89 (95% CI, 0.81-0.94) performs slightly superior compared to these studies. The most recent performance, using a CNN-based method, [19] achieved a Dice score of 0.63 ± 0.16 and an ICC of 0.966 in a test set of 473 patients. The authors extracted the intracranial region prior to training of their best performing network, reducing complexity. Interestingly, the authors achieved a Dice score of 0.40 with a reduced UNet architecture on their dataset. Moreover, our performance compares strongly to the 0.64 interobserver Dice score that is found between two experienced radiologists [19,40]. This emphasizes the added value of a more complex model and data augmentation in the segmentation of aSAH without any additional preprocessing in a relatively small training set.

We currently still lack a reliable surrogate marker to identify those patients who develop SAH-SBI after aSAH. Established clinical [20,21] and radiological scores [22–24] were shown to have limited predictive accuracy for SAH-SBI [41,42] other than functional outcome [43], which is supported by our study. In addition, these scores are associated with substantial intra- and interrater variability [44]. Transcranial doppler ultrasonography is widely used to monitor for aVSP after aSAH, but it is associated with poor interrater reliability and low sensitivity and negative predictive values for SAH-SBI. [7,45–47] Although several serum parameters have been described and proposed, none have proven to be a robust predictor for SAH-SBI [48,49]. CSF-Hb was shown to be a mechanistic driver for SAH-SBI and a promising monitoring biomarker. [7,8,12,16,50] A prospective single-center pilot study indicated a high discriminatory ability of this method for SAH-SBI (AUC = 0.89 [0.85-0.92]) [7]. Measuring CSF-Hb levels, however, requires a CSF access device. Thus, there is a clinical need for a non-invasive alternative in patients without external ventricular drain or lumbar drain. There is a plausible pathophysiological cascade between the volume of blood released by aSAH (ISHV), the number of lysing erythrocytes in the subarachnoid space, and CSF-Hb levels [7]. Despite this pathophysiological plausibility, our study showed that ISHV is an insufficient surrogate marker for SAH-SBI. A possible explanation for the low discriminatory ability with simultaneous strong association between ISHV and SAH-SBI is that CSF-Hb is released from the subarachnoid blood clot at individual dynamics, determined by RBC-intrinsic characteristic driving erythrolysis, and the RBC clearance capacity of hematoma-associated phagocytes [7,51]. Such dynamics determine the attainment of critical thresholds for the occurrence of aVSP, DCI, and DIND at a given time point [7]. Thus, monitoring CSF-Hb levels by regular CSF sampling via an external ventricular drain or lumbar drain addresses the pathophysiological cascade more distally and might be more suitable for this purpose.

ISHV showed a high discriminatory ability for ventriculoperitoneal shunt dependence and functional outcome at three-months follow-up, and independent association with survival. These findings may be explained by the fact that these medium- and long-term effects are not only determined by reaching CSF-Hb thresholds at a specific time point, but also reflect the temporally integrated toxic effect of cell-free hemoglobin and its downstream products on brain parenchyma [11,52–55]. The individual differences in these dynamics could facilitate ISHV in contributing to superiority over existing simplified radiological scales, due to the highly patient specific readout.

Our study is subject to several limitations. First, CT data on which ISHV determination is based were not acquired on the same scanner,

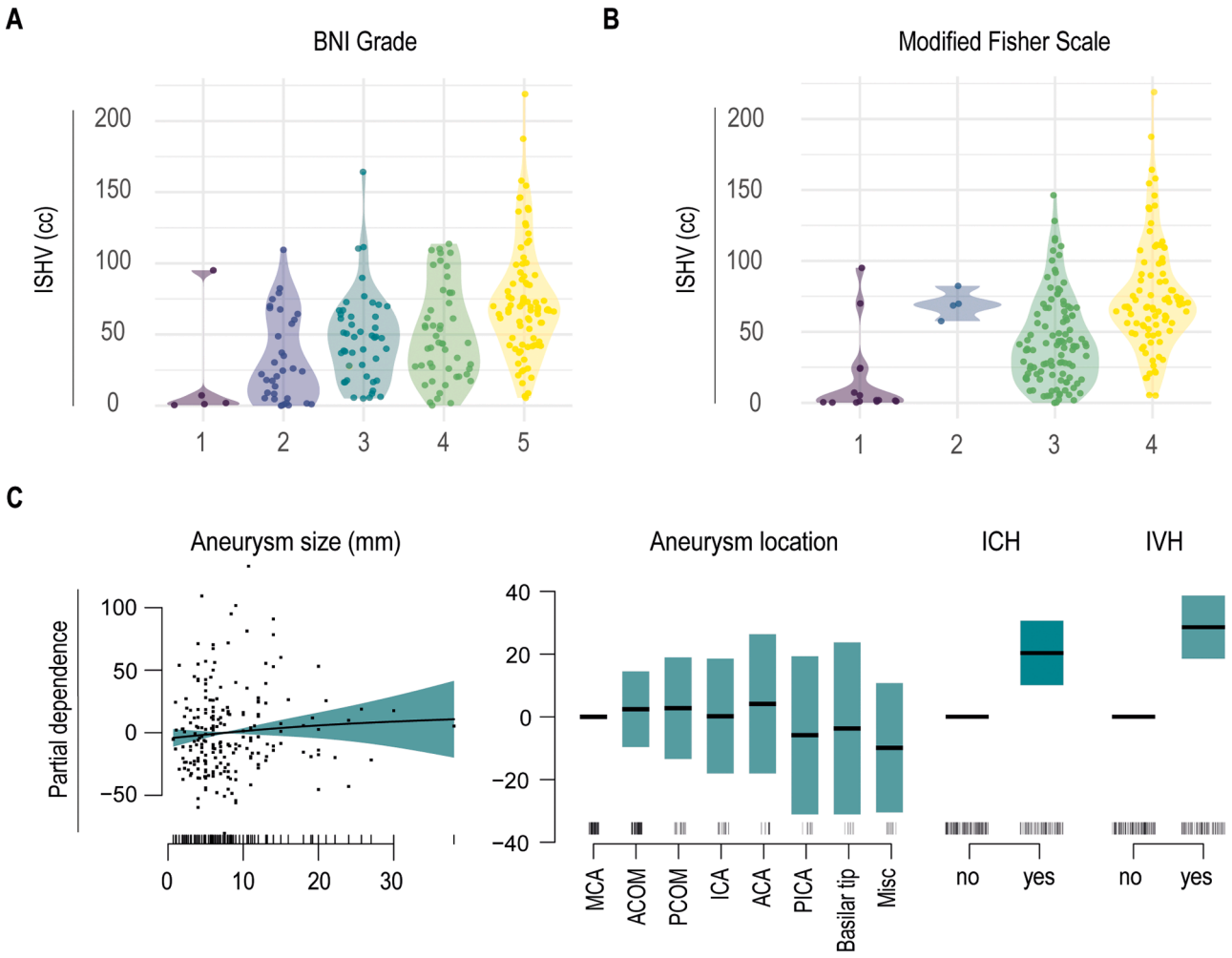

Fig. 5. Initial subarachnoid hematoma volume and radiological baseline features. Initial subarachnoid hematoma volume (ISHV) stratified by Barrow Neurological Institute (BNI) grade (**A**) and Modified Fisher Scale (**B**). (**C**) Partial dependence of ISHV on aneurysm size, aneurysm location (MCA, middle cerebral artery; ACOM, anterior communicating artery; PCOM, posterior communicating artery; ICA, internal carotid artery; ACA, anterior cerebral artery; PICA, posterior inferior cerebellar artery; Misc, miscellaneous), intracerebral hemorrhage (ICH), and intraventricular hemorrhage (IVH).

Table 3
Overall incidence of aneurysmal subarachnoid hemorrhage-related secondary brain injury (SAH-SBI), angiographic vasospasms (aVSP), delayed cerebral ischemia (DCI), delayed ischemic neurological deficits (DIND), and the need for spasmolysis.

Total *n*	220
SAH-SBI [*n* (%)]	123 (55.9)
aVSP [*n* (%)]	122 (55.5)
DCI [*n* (%)]	52 (23.6)
DIND [*n* (%)]	39 (17.7)
Spasmolysis [*n* (%)]	36 (16.4)

instead the initial CT image of the patient was used, which in part also originated from referring centers. The use of different CT scanners and different imaging protocols introduced some heterogeneity into the dataset. However, this heterogeneity strengthens the robustness of our algorithm, which was thus trained and tested in a clinically realistic setting. Second, the dataset that was used for training and validation of our segmentation algorithm could be further expanded, since the performance of deep learning models increases with larger datasets [56]. In a hybrid 2D/3D study [57], a total of 11,021 scans were used for development and validation resulting in a Dice score of 0.77 for aSAH segmentation. Moreover, those authors included other variants of intracranial hemorrhage, enabling the algorithm to differentiate between different types of intracranial hemorrhages. Our algorithm is expectedly not suitable for quantifying intracranial hemorrhages other than aSAH.

Conclusion

Without any additional preprocessing, we demonstrated strong performance of our CNN in volumetric segmentation of aSAH in the admission CT. The automatically segmented ISHV has shown a high discriminatory ability for ventriculoperitoneal shunt dependence and functional outcome at three-months follow-up. Moreover, there was strong evidence for a negative association between survival probability and ISHV. The discriminatory ability of ISHV for SAH-SBI, however, was similar to established clinical and radiological scores. Interindividual differences in CSF-Hb releasing dynamics from the subarachnoid blood clot may explain the limited discriminatory value of ISHV for SAH-SBI, deeming ISHV insufficient as surrogate marker for CSF-Hb.

Ethical approval and consent to participate

This study was approved by the ethical review board of the Canton of Zurich, Switzerland (KEK ZH 2021-01844). A written general consent for further use of their patient-specific data has been obtained from all

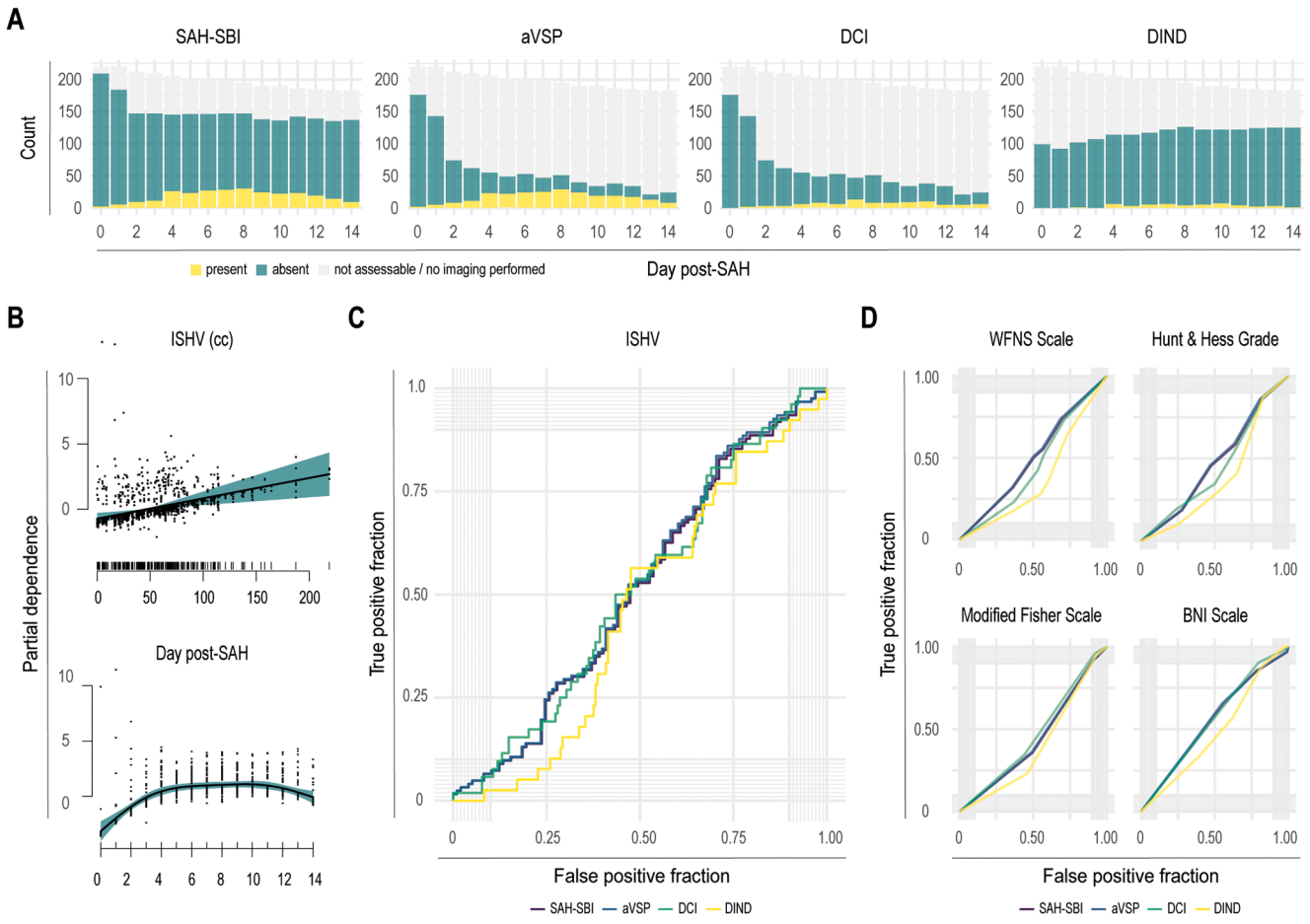

Fig. 6. Epidemiology and associations of subarachnoid hemorrhage-related secondary brain injury. (**A**) Count data on subarachnoid hemorrhage-related secondary brain injury (SAH-SBI), angiographic vasospasms (aVSP), delayed cerebral ischemia (DCI), and delayed ischemic neurological deficits (DIND) stratified by day post-SAH. (**B**) Partial dependence of SAH-SBI on the initial subarachnoid hematoma volume (ISHV) and the day post-SAH. (**C**) Receiver operating characteristic (ROC) curves of the ISHV for SAH-SBI, aVSP, DCI, and DIND. (**D**) ROC curves of established clinical (World Federation of Neurosurgical Societies (WFNS), Hunt & Hess) and radiological scores (Modified Fisher, Barrow Neurological Institute (BNI)) for SAH-SBI, aVSP, DCI, and DIND.

Table 4
Diurnal incidence of aneurysmal subarachnoid hemorrhage-related secondary brain injury (SAH-SBI), angiographic vasospasms (aVSP), delayed cerebral ischemia (DCI), and delayed ischemic neurological deficits (DIND).

Total of assessed days *n*	2979
Diurnal assessment of SAH-SBI [*n* (%)]	
No SAH-SBI	1973 (66.2)
SAH-SBI detectable	272 (9.1)
SAH-SBI evaluation not possible	734 (24.6)
Diurnal assessment of aVSP [*n* (%)]	
Days with no aVSP detectable imaging	652 (21.9)
Days with aVSP detectable on imaging	248 (8.3)
Days without imaging	2078 (69.8)
Diurnal assessment of DCI [*n* (%)]	
Days with no DCI detectable on imaging	809 (27.2)
Days with DCI detectable on imaging	91 (3.1)
Days without imaging	2078 (69.8)
Diurnal assessment of DIND [*n* (%)]	
No DIND	1686 (56.6)
DIND	47 (1.6)
DIND not assessable	1246 (41.8)

Table 5
Discriminatory ability (area under the receiver operating characteristic curve with 95% confidence interval) of established clinical (World Federation of Neurosurgical Societies (WFNS), Hunt & Hess) and radiological (modified Fisher, Barrow Neurological Institute (BNI)) scores for subarachnoid hemorrhage-related secondary brain injury (SAH-SBI), angiographic vasospasms (aVSP), delayed cerebral ischemia (DCI), and delayed ischemic neurological deficits (DIND).

	SAH-SBI	aVSP	DCI	DIND
WFNS score	0.50 (0.42-0.57)	0.50 (0.43-0.58)	0.45 (0.37-0.54)	0.38 (0.29-0.47)
Hunt & Hess score	0.47 (0.40-0.55)	0.48 (0.41-0.56)	0.45 (0.37-0.54)	0.39 (0.30-0.48)
Modified Fisher scale	0.44 (0.37-0.51)	0.44 (0.38-0.51)	0.47 (0.39-0.55)	0.40 (0.32-0.48)
BNI score	0.55 (0.47-0.62)	0.55 (0.48-0.62)	0.55 (0.47-0.64)	0.48 (0.39-0.57)

patients or their legal representatives.

Consent for publication

All authors have read and approved the submitted manuscript.

Availability of supporting data

The anonymized dataset and all code (Python and R) will be made available online (https://doi.org/10.5281/zenodo.7443202). The use of dynamic reporting guarantees full reproducibility of the results.

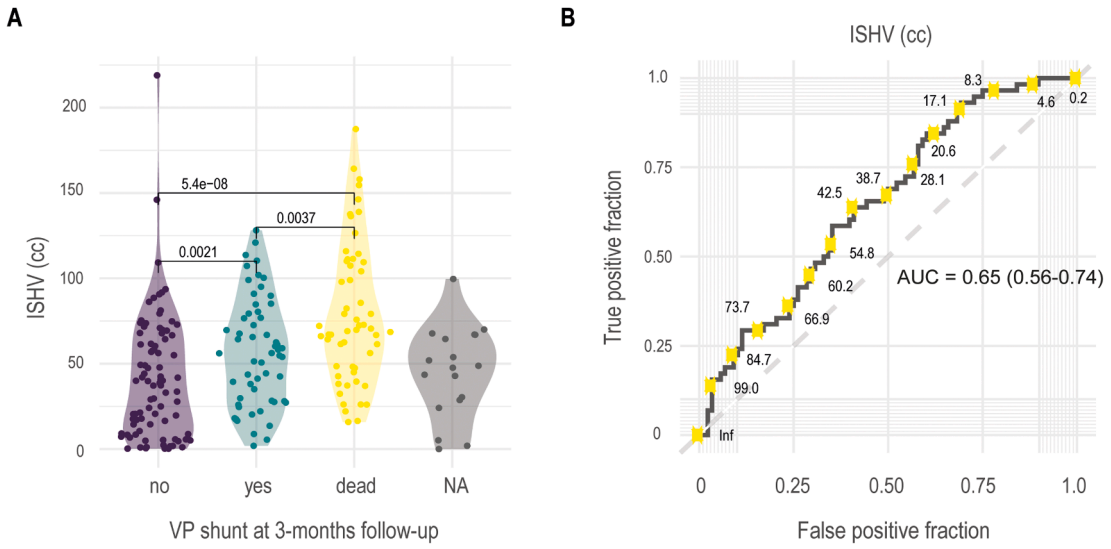

Fig. 7. Initial subarachnoid hematoma volume and ventriculoperitoneal shunt dependence. (**A**) Initial subarachnoid hematoma volume (ISHV) stratified by ventriculoperitoneal (VP) shunt dependence at three-months follow-up. (**B**) Receiver operating characteristic curve and area under the curve (AUC) of the ISHV for ventriculoperitoneal shunt dependence at three-months follow-up.

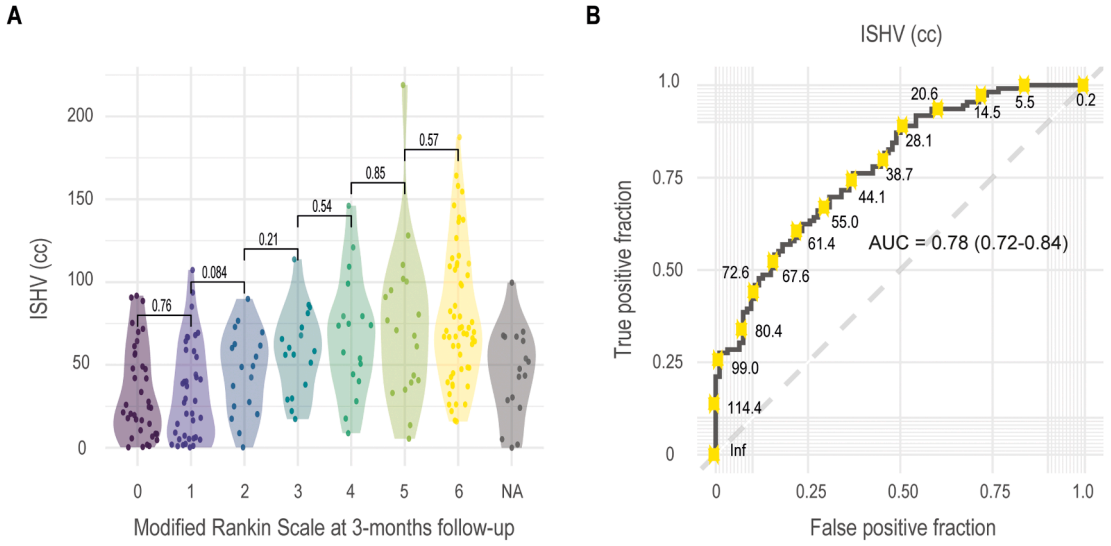

Fig. 8. Initial subarachnoid hematoma volume and functional status after three months. (**A**) Initial subarachnoid hematoma volume (ISHV) stratified by modified Rankin Scale at three-months follow-up. (**B**) Receiver operating characteristic curve and area under the curve (AUC) of the ISHV discriminating between a good (0-2) and a poor (3-6) mRS at three-months follow-up.

Authors' information

Not applicable.

CRediT authorship contribution statement

Bart R Thomson: Conceptualization, Methodology, Writing – original draft, Writing – review & editing. **Firat Gürlek:** Conceptualization, Methodology, Writing – original draft, Writing – review & editing. **Raphael M Buzzi:** Methodology, Funding acquisition, Writing – review & editing. **Nina Schwendinger:** Methodology, Writing – review & editing. **Emanuela Keller:** Methodology, Writing – review & editing. **Luca Regli:** Methodology, Project administration, Writing – review & editing. **Tristan PC van Doormaal:** Methodology, Writing – review & editing. **Dominik J Schaer:** Conceptualization, Methodology, Funding acquisition, Project administration, Supervision, Writing – review & editing. **Michael Hugelshofer:** Conceptualization, Methodology, Funding acquisition, Project administration, Supervision, Writing – review & editing. **Kevin Akeret:** Conceptualization, Methodology, Funding acquisition, Project administration, Supervision, Writing – original draft, Writing – review & editing.

Declaration of Competing Interest

The authors declare the following financial interests/personal relationships which may be considered as potential competing interests:

Raphael M Buzzi reports financial support was provided by Swiss National Science Foundation. Dominik J Schaer reports financial support was provided by Swiss National Science Foundation. Michael Hugelshofer reports financial support was provided by Swiss National Science Foundation. Dominik Schaer reports was provided by Innosuisse Swiss Innovation Agency. Kevin Akeret reports was provided by Uniscientia Foundation. Raphael M Buzzi reports was provided by University of Zurich. Kevin Akeret reports financial support was provided by

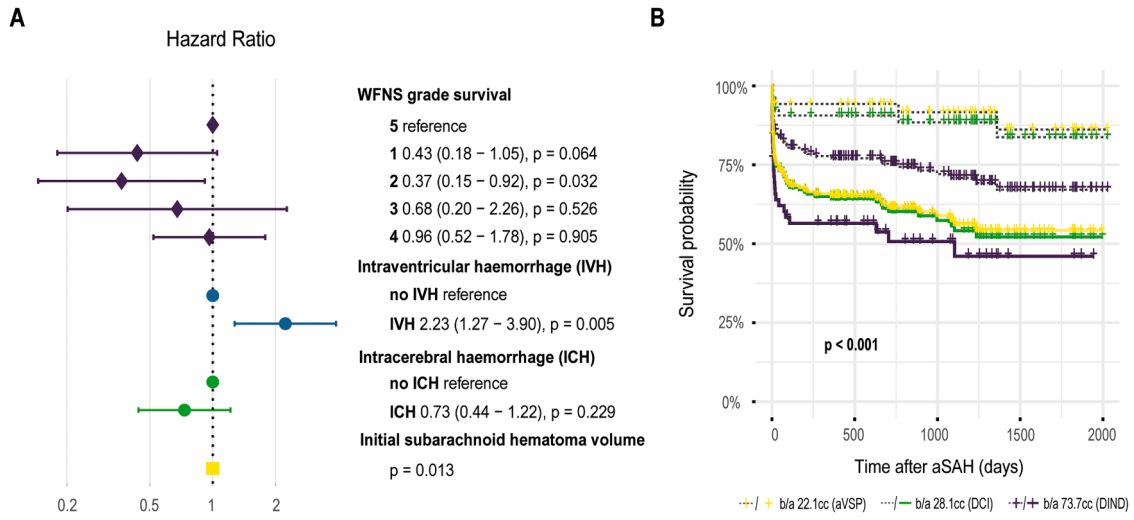

Fig. 9. Survival after aneurysmal subarachnoid hemorrhage. (**A**) Multivariate survival analysis (Cox proportional hazards regression model) considering World Federation of Neurosurgical Societies (WFNS, violet) grade, presence of intraventricular (IVH, blue) or intracerebral (ICH, green) hemorrhage, and initial subarachnoid hematoma volume (ISHV, yellow). (**B**) Survival probability stratified by the optimal discriminatory (below and above (b/a) optimal Youden indices) of ISHV for angiographic vasospasms (aVSP, yellow), delayed cerebral ischemia (DCI, green), and delayed ischemic neurological deficits (DIND, violet), visualized using the Kaplan Meier method.

University of Zurich. Tristan PC van Doormaal reports a relationship with AugmedIT B.V. that includes: board membership.

Acknowledgments

Not applicable.

References

1 Rincon F, Rossenwasser RH, Dumont A. The epidemiology of admissions of nontraumatic subarachnoid hemorrhage in the United States. *Neurosurgery*. 2013;73:217–222. discussion 212-3.
2 Etminan N, Chang H-S, Hackenberg K, De Rooij NK, Vergouwen MDI, Rinkel GJE, et al. Worldwide incidence of aneurysmal subarachnoid hemorrhage according to region, time period, blood pressure, and smoking prevalence in the population: a systematic review and meta-analysis. *JAMA Neurol*. 2019;76:588–597.
3 Sehba FA, Hou J, Pluta RM, Zhang JH. The importance of early brain injury after subarachnoid hemorrhage. *Prog Neurobiol*. 2012;97:14–37.
4 Macdonald RL. Delayed neurological deterioration after subarachnoid haemorrhage. *Nat Rev Neurol*. 2014;10:44–58.
5 Dorsch NWC, King MT. A review of cerebral vasospasm in aneurysmal subarachnoid haemorrhage Part I: incidence and effects. *J Clin Neurosci*. 1994;1:19–26.
6 Rowland MJ, Hadjipavlou G, Kelly M, Westbrook J, Pattinson KTS. Delayed cerebral ischaemia after subarachnoid haemorrhage: looking beyond vasospasm. *Br J Anaesth*. 2012;109:315–329.
7 Akeret K, Buzzi RM, Schaer CA, Thomson BR, Vallelian F, Wang S, et al. Cerebrospinal fluid hemoglobin drives subarachnoid hemorrhage-related secondary brain injury. *J Cereb Blood Flow Metab*. 2021 Jun 8.
8 Hugelshofer M, Buzzi RM, Schaer CA, Richter H, Akeret K, Anagnostakou V, et al. Haptoglobin administration into the subarachnoid space prevents hemoglobin-induced cerebral vasospasm. *J Clin Invest*. 2019;129:5219–5235.
9 Buzzi RM, Owczarek CM, Akeret K, Tester A, Pereira N, Butcher R, et al. Modular platform for the development of recombinant hemoglobin scavenger biotherapeutics. *Mol Pharm*. 2021;18:3158–3170.
10 Garland P, Morton M, Zolnourian A, Durnford A, Gaastra B, Toombs J, et al. Neurofilament light predicts neurological outcome after subarachnoid haemorrhage. *Brain*. 2021;144:761–768.
11 Buzzi RM, Akeret K, Schwendinger N, Klohs J, Vallelian F, Hugelshofer M, et al. Spatial transcriptome analysis defines heme as a hemopexin-targetable inflammatoxin in the brain. *Free Radic Biol Med* https://doi.org/10.1016/j.freeradbiomed.2021.11.011.
12 Hugelshofer M, Sikorski CM, Seule M, Deuel J, Muroi CI, Seboek M, et al. Cell-free oxyhemoglobin in cerebrospinal fluid after aneurysmal subarachnoid hemorrhage: biomarker and potential therapeutic target. *World Neurosurg*. 2018;120:e660–e666.
13 Andersen CBF, Torvund-Jensen M, Nielsen MJ, de Oliveira CLP, Hersleth H-P, Andersen NH, et al. Structure of the haptoglobin-haemoglobin complex. *Nature*. 2012;489:456–459.
14 Buehler PW, Humar R, Schaer DJ. Haptoglobin therapeutics and compartmentalization of cell-free hemoglobin toxicity. *Trends Mol Med*. 2020;26:683–697.
15 Vallelian F, Buehler PW, Schaer DJ. Hemolysis, free hemoglobin toxicity, and scavenger protein therapeutics. *Blood*. 2022;140:1837–1844.
16 Akeret K, Buzzi RM, Saxenhofer M, Bieri K, Chiavi D, Thomson BR, et al. The HeMoVal study protocol: a prospective international multicenter cohort study to validate cerebrospinal fluid hemoglobin as a monitoring biomarker for aneurysmal subarachnoid hemorrhage related secondary brain injury. *BMC Neurol*. 2022;22:267.
17 Prakash KNB, Zhou S, Morgan TC, Hanley DF, Nowinski WL. Segmentation and quantification of intra-ventricular/cerebral hemorrhage in CT scans by modified distance regularized level set evolution technique. *Int J Comput Assist Radiol Surg*. 2012;7:785–798.
18 Litjens G, Kooi T, Bejnordi BE, Setio AAA, Ciompi F, Ghafoorian M, et al. A survey on deep learning in medical image analysis. *Med Image Anal*. 2017;42:60–88.
19 Barros RS, van der Steen WE, Boers AMM, Zijlstra I, van den Berg R, El Youssoufi W, et al. Automated segmentation of subarachnoid hemorrhages with convolutional neural networks. *Inform Med Unlocked*. 2020;19, 100321.
20 Teasdale GM, Drake CG, Hunt W, Kassell N, Sano K, Pertuiset B, et al. A universal subarachnoid hemorrhage scale: report of a committee of the World Federation of neurosurgical societies. *J Neurol Neurosurg Psychiatry*. 1988;51:1457.
21 Hunt WE, Hess RM. Surgical risk as related to time of intervention in the repair of intracranial aneurysms. *J Neurosurg*. 1968;28:14–20.
22 Wilson DA, Nakaji P, Abla AA, Uschold TD, Fusco DJ, Oppenlander ME, et al. A simple and quantitative method to predict symptomatic vasospasm after subarachnoid hemorrhage based on computed tomography: beyond the Fisher scale. *Neurosurgery*. 2012;71:869–875.
23 Fisher CM, Kistler JP, Davis JM. Relation of cerebral vasospasm to subarachnoid hemorrhage visualized by computerized tomographic scanning. *Neurosurgery*. 1980;6:1–9.
24 Frontera JA, Claassen J, Schmidt JM, Wartenberg KE, Temes R, Connolly Jr ES, et al. Prediction of symptomatic vasospasm after subarachnoid hemorrhage: the modified fisher scale. *Neurosurgery*. 2006;59:21–27. discussion 21-7.
25 von Elm E, E von Elm, Altman DG, Egger M, Pocock SJ, Gøtzsche PC, et al. The strengthening the reporting of observational studies in epidemiology (STROBE) statement. *Epidemiology*. 2007;18:800–804.
26 Kerfoot E, Clough J, Oksuz I, Lee J, King AP, Schnabel JA. Left-ventricle quantification using residual U-net. statistical atlases and computational models of the heart. atrial segmentation and LV quantification challenges. *Springer Int Publish*. 2019:371–380.
27 The MONAI Consortium. *Project MONAI*. 2020.
28 Wood SN. *Generalized Additive Models: An Introduction with R, Second Edition*. CRC Press; 2017.
29 Sing T, Sander O, Beerenwinkel N, Lengauer T. ROCR: visualizing classifier performance in R. *Bioinformatics*. 2005;21:3940–3941.
30 Sachs MC. plotROC: a tool for plotting ROC curves. *J Stat Softw*. 2017:79.
31 Robin X, Turck N, Hainard A, Tiberti N, Lisacek F, Sanchez J-C, et al. pROC: an open-source package for R and S to analyze and compare ROC curves. *BMC Bioinformatics*. 2011;12.
32 Khan MRAA. ROCit- An R package for performance assessment of binary classifier with visualization. 2019.
33 Therneau T. A package for survival analysis in R. R package version 2020;3:1–12.
34 Borgan Ø. Modeling survival data: Extending the cox model. Terry M. therneau and Patricia M. grambsch, Springer-Verlag, New York, 2000. No. Of pages: Xiii + 350. Price: $69.95. ISBN 0-387-98784-3. *Stat Med* 2001;20:2053–2054.
35 Bland M. *An Introduction to Medical Statistics*. Oxford University Press; 2015.

36 Cosic D, Loucaric S. Computer system for quantitative: analysis of ICH from CT head images. In: *Proceedings of the 19th Annual International Conference of the IEEE Engineering in Medicine and Biology Society. "Magnificent Milestones and Emerging Opportunities in Medical Engineering" (Cat. No.97CH36136)*. 2. 1997:553–556. ieee xplore.ieee.org. vol.2.

37 Bardera A, Boada I, Feixas M, Remollo S, Blasco G, Silva Y, et al. Semi-automated method for brain hematoma and edema quantification using computed tomography. *Comput Med Imaging Graph*. 2009;33:304–311.

38 Bhadauria HS, Singh A, Dewal ML. An integrated method for hemorrhage segmentation from brain CT Imaging. *Comput Electr Eng*. 2013;39:1527–1536.

39 Shahangian B, Pourghassem H. Automatic brain hemorrhage segmentation and classification algorithm based on weighted grayscale histogram feature in a hierarchical classification structure. *Biocybernet Biomed Eng*. 2016;36:217–232.

40 Boers AM, Zijlstra IA, Gathier CS, van den Berg R, Slump CH, Marquering HA, et al. Automatic quantification of subarachnoid hemorrhage on noncontrast CT. *AJNR Am J Neuroradiol*. 2014;35:2279–2286.

41 Rosen DS, Macdonald RL. Grading of subarachnoid hemorrhage: modification of the world World Federation of Neurosurgical Societies scale on the basis of data for a large series of patients. *Neurosurgery*. 2004;54:566–575. discussion 575-6.

42 van der Steen WE, Leemans EL, van den Berg R, Roos YBWEM, Marquering HA, Verbaan D, et al. Radiological scales predicting delayed cerebral ischemia in subarachnoid hemorrhage: systematic review and meta-analysis. *Neuroradiology*. 2019;61:247–256.

43 Jaja BNR, Saposnik G, Lingsma HF, Macdonald E, Thorpe KE, Mamdani M, et al. Development and validation of outcome prediction models for aneurysmal subarachnoid haemorrhage: the SAHIT multinational cohort study. *BMJ*. 2018 Jan 18.

44 Degen LAR, Dorhout Mees SM, Algra A, Rinkel GJE. Interobserver variability of grading scales for aneurysmal subarachnoid hemorrhage. *Stroke*. 2011;42:1546–1549.

45 Lysakowski C, Walder B, Costanza MC, Tramèr MR. Transcranial Doppler versus angiography in patients with vasospasm due to a ruptured cerebral aneurysm: A systematic review. *Stroke*. 2001;32:2292–2298.

46 Krejza J, Szydlik P, Liebeskind DS, Kochanowicz J, Bronov O, Mariak Z, et al. Age and sex variability and normal reference values for the VMCA/VICA index. *AJNR Am J Neuroradiol*. 2005;26:730–735.

47 Naval NS, Thomas CE, Urrutia VC. Relative changes in flow velocities in vasospasm after subarachnoid hemorrhage: a transcranial Doppler study. *Neurocrit Care*. 2005;2:133–140.

48 Zheng Y-K, Dong X-Q, Du Q, Wang H, Yang D-B, Zhu Q, et al. Comparison of plasma copeptin and multiple biomarkers for assessing prognosis of patients with aneurysmal subarachnoid hemorrhage. *Clin Chim Acta*. 2017;475:64–69.

49 Jung CS, Lange B, Zimmermann M. Seifert V. CSF and serum biomarkers focusing on cerebral vasospasm and ischemia after subarachnoid hemorrhage. *Stroke Res Treat*. 2013;2013, 560305.

50 Thomson BR, Richter H, Akeret K, Buzzi RM, Anagnostakou V, van Niftrik CHB, et al. Blood oxygenation-level dependent cerebrovascular reactivity imaging as strategy to monitor CSF-hemoglobin toxicity. *J Stroke Cerebrovasc Dis*. 2023;32:106985.

51 Humar R, Schaer DJ, Vallelian F. Erythrophagocytes in hemolytic anemia, wound healing, and cancer. *Trends Mol Med*. 2022;28:906–915.

52 Garland P, Morton MJ, Haskins W, Zolnourian A, Durnford A, Gaastra B, et al. Haemoglobin causes neuronal damage in vivo which is preventable by haptoglobin. *Brain Commun*. 2020;2:fcz053.

53 Galea I, Durnford A, Glazier J, Mitchell S, Kohli S, Foulkes L, et al. Iron deposition in the brain after aneurysmal subarachnoid hemorrhage. *Stroke*. 2022;53:1633–1642.

54 Bücker P, Buzzi RM, Akeret K, Mosberger L, Richter H, Sperling M, et al. A model to visualize the fate of iron after intracranial hemorrhage using isotopic tracers and elemental bioimaging. *Metallomics*. 2022;14.

55 Akeret K, Buzzi RM, Thomson BR, Schwendinger N, Klohs J, Schulthess-Lutz N, et al. MyD88-TLR4-dependent choroid plexus activation precedes perilesional inflammation and secondary brain edema in a mouse model of intracerebral hemorrhage. *J Neuroinflammation*. 2022;19:290.

56 Esteva A, Robicquet A, Ramsundar B, Kuleshov V, DePristo M, Chou K, et al. A guide to deep learning in healthcare. *Nat Med*. 2019;25:24–29.

57 Chang PD, Kuoy E, Grinband J, Weinberg BD, Thompson M, Homo R, et al. Hybrid 3D/2D convolutional neural network for hemorrhage evaluation on head CT. *AJNR Am J Neuroradiol*. 2018;39:1609–1616.

58 Iqbal H. HarisIqbal88/PlotNeuralNet v1.0.0. 2018.